Smart dual-sensor wound dressing for monitoring cutaneous wounds

Bahram Mirani, Zhina Hadisi, Erik Pagan, Seyed Mohammad Hossein Dabiri, Antonia van Rijt, Lama Almutairi, Iman Noshadi, David G. Armstrong, and Mohsen Akbari

2023

ADVANCED HEALTHCARE MATERIALS
www.advhealthmat.de

Smart Dual-Sensor Wound Dressing for Monitoring Cutaneous Wounds

*Bahram Mirani, Zhina Hadisi, Erik Pagan, Seyed Mohammad Hossein Dabiri, Antonia van Rijt, Lama Almutairi, Iman Noshadi, David G. Armstrong, and Mohsen Akbari**

Managing slow-healing wounds and associated complications is challenging, time-consuming, and expensive. Systematic collection, analysis, and dissemination of correct wound status data are critical for enhancing healing outcomes and reducing complications. However, traditional data collection approaches are often neither accurate nor user-friendly and require diverse skill levels, resulting in the collection of inconsistent and unreliable data. As an advancement to the authors' previously developed hydrogel-based smart wound dressing, here is reported an enhanced integration of drug delivery and sensing (pH and glucose) modules for accelerated treatment and continuous monitoring of cutaneous wounds. In the current study, growth factor delivery modules and an array of colorimetric glucose sensors are incorporated into the dressing to promote wound healing and extend the dressing's utility for diabetic wound treatment. Furthermore, the efficacy of the wound dressing in monitoring infection and supporting wound healing via antibiotic and growth factor delivery is investigated in mice models. The updated dressing reveals excellent healing benefits on non-infected and infected wounds, as well as real-time monitoring and early detection of wound infection.

1. Introduction

Wound management is one of the most resource-intensive medical care processes and has become an increasing healthcare challenge, globally.[1] Reports have shown that around 6.5 million people at a time live with chronic wounds in the US alone, entailing an annual expenditure of more than US$25 billion.[2] The prevalence of chronic wounds has an increasing trend owing to the population aging and longer life-expectancy.[3,4] Wound complications such as infection, tissue necrosis, dehiscence, and cellulitis cause mortality or delay wound healing resulting in prolonged hospitalization and increased treatment cost.[5] Among these complications, infection is a major cause of severe medical conditions, amputation, or death, namely, accounting for about 75% of mortality in burn victims.[6]

While effective wound care necessitates constant wound screening and early diagnosis of wound complications such as infection, current clinical methods—mostly based on the analysis of wound specimens—do not easily accommodate real-time wound monitoring, leaving the management of acute and chronic wounds a major challenge.[6] Alternatively, in situ wound monitoring has recently been realized via the incorporation of flexible electronics or colorimetric sensors into wound dressings to respond to various biomarkers such as pH,[7–9] temperature,[9,10] oxygen levels,[11,12] glucose concentration,[13] and microorganisms' by-products[14–17] that serve as indicators of the wound status.

B. Mirani, Z. Hadisi, E. Pagan, S. M. H. Dabiri, A. van Rijt, L. Almutairi, M. Akbari
Laboratory for Innovations in Microengineering (LiME)
Department of Mechanical Engineering
University of Victoria
Victoria, BC V8P 5C2, Canada
E-mail: makbari@uvic.ca

The ORCID identification number(s) for the author(s) of this article can be found under https://doi.org/10.1002/adhm.202203233

DOI: 10.1002/adhm.202203233

B. Mirani, Z. Hadisi, E. Pagan, S. M. H. Dabiri, M. Akbari
Center for Advanced Materials and Related Technologies (CAMTEC)
University of Victoria
Victoria, BC V8P 5C2, Canada

I. Noshadi
Department of Bioengineering
University of California
Riverside, CA 92507, USA

D. G. Armstrong
Southwestern Academic Limb Salvage Alliance (SALSA)
Department of Surgery
Keck School of Medicine of University of Southern California
Los Angeles, CA 90033, USA

M. Akbari
Terasaki Institute for Biomedical Innovation
Los Angeles, CA 90064, USA

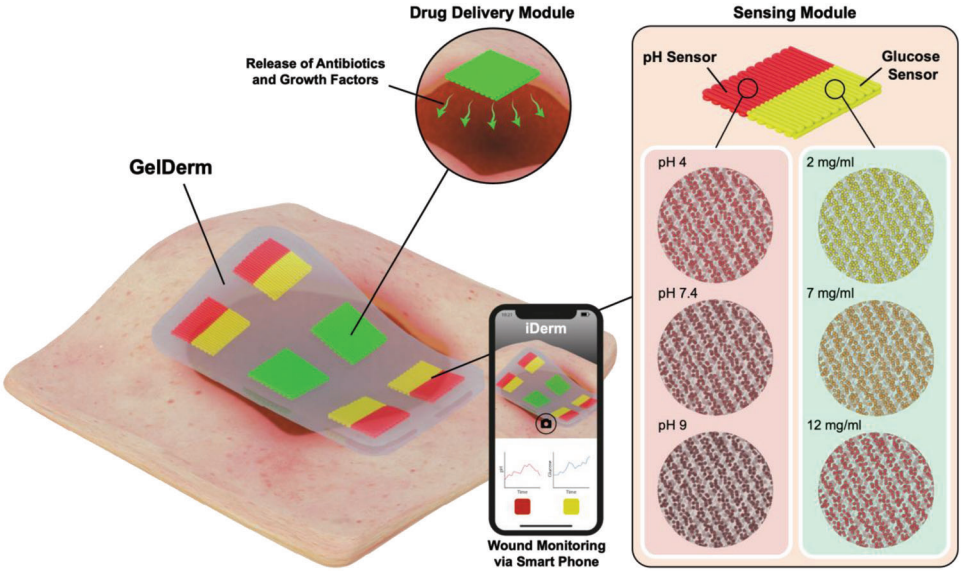

Figure 1. Schematic of GelDerm showing its integrated arrays of drug-releasing and sensing modules. Sensing modules are alginate hydrogel-based, 3D printed components containing pH and glucose sensing microparticles, capable of real-time detection of bacterial infection and monitoring of glucose levels in the wound environment. iDerm, a developed smartphone application, wirelessly monitors infection and glucose levels by imaging and analyzing GelDerm's colorimetric sensors.

Wireless communication between these integrated sensors and screening platforms such as smartphone applications has given rise to a new generation of wound dressings that enables real-time and remote monitoring of the physicochemical properties of the wound.[18–20] In comparison with electrochemical systems, colorimetric sensors have recently attracted great attention because they do not need electrical circuitry and power source and, especially, do not require electric conductivity, which can be a source of cytotoxicity.[17] While these wound dressings have a great potential to considerably reduce mortality, hospitalization, cost, and labor in wound care, further steps are still required to put them into clinical practice.

In addition to wound monitoring, in situ delivery of therapeutic agents such as growth factors is essential to accelerate the healing of chronic wounds.[21] As a complex biological cascade, wound healing depends on cellular proliferation and differentiation, chemotaxis, secretion of the extracellular matrix (ECM), neovascularization, and tissue remodeling. Among various types of growth factors, basic fibroblast growth factor (bFGF) and vascular endothelial growth factor (VEGF) have been shown to regulate these biological processes. It has extensively been reported that bFGF induces fibroblast and keratinocyte proliferation and migration, collagen deposition, reepithelialization, and the formation of granulation tissue.[22–25] VEGF has been shown to stimulate wound healing via the upregulation of angiogenesis.[21,26,27] Encapsulation of these growth factors into wound dressings provides the sustained delivery of these agents while slowing their enzymatic degradation.[22,28]

Herein, further advancements and in vivo study of a previously developed hydrogel wound dressing—with the capability to detect wound infection, monitor glucose level, and deliver antibiotics and growth factors at the wound site—are presented.[7,8,29] The wound dressing, patented as GelDerm, detects and maps bacterial infection based on the change in the pH of the wound using an array of colorimetric pH sensors. Notably, the previously established capabilities of GelDerm have been echoed and compared to those of other wound dressings in several recent review articles.[30–34] In the present study, the detection capacity and precision of these pH sensors were assessed under various temperature and storage-time conditions. To better aid wound healing in patients suffering from chronic diabetic wounds, an array of glucose sensors was developed and incorporated into the wound dressing to monitor the glucose concentration at the wound site in a real-time fashion (**Figure 1**). In addition to improvements in wound monitoring, growth-factor-releasing components were integrated with GelDerm to accelerate wound healing. Furthermore, GelDerm's ability in infection sensing and therapeutic agent delivery was evaluated in non-infected and infected wounds in mouse models.

2. Results and Discussion

2.1. Physical Characterization of GelDerm

Wound dressings were fabricated using three types of commercially available alginate polymers with low and high viscosity and different M/G ratios. As shown in Figure S1, Supporting Information, dressings made of alginic acid sodium salt with medium viscosity (15–25 cP, 1 wt.% in H_2O at 25 °C, and M/G ratio of 0.43) showed the highest viscoelastic metrics—loss and storage modulus—as well as better mechanical performance by exhibiting higher elastic modulus, ultimate stress, and toughness. While having higher toughness, which is essential for the endurance of the dressing on the wound, these dressings showed a similar degree of elongation ($p = 0.5538$) as other groups, demonstrating higher mechanical stability with extensibility similar to that of softer alginate hydrogels. Additionally, the water vapor transmission (WVR) properties, swelling behavior in media with

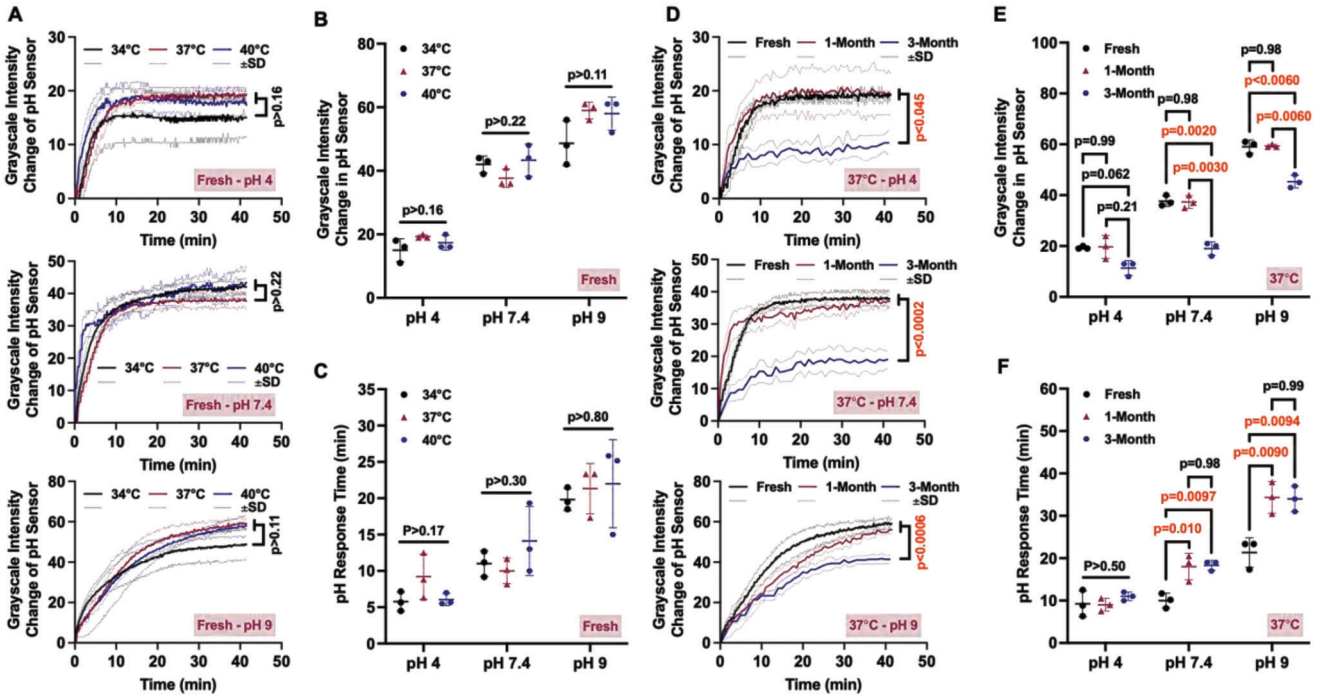

Figure 2. The impact of temperature changes and storage time on the performance of the wound dressing. A) Change in the grayscale intensity of the pH sensor with time at temperatures from 34 to 37 °C when exposed to buffer solutions with pH values ranging from 4 to 9. B,C) Comparing the grayscale intensity change (B) and response time (C) of the pH sensors at temperatures from 34 to 37 °C in various pH values. D) Change in the grayscale intensity of the pH sensor with 3 different storage time conditions—fresh, 1-month old, and 3-month old—with time. E,F) Comparing the grayscale intensity change (E) and the response time (F) of the pH sensors in fresh, 1-month-old, and 3-month-old conditions. In (A) and (D), solid lines show the mean values and fade dash lines show ± SD for their associated colors. Error bars show mean ±SD. N = 3.

different acidities, and degradation of GelDerm were characterized as presented in Figure S2, Supporting Information.

2.2. Wound Screening Performance of GelDerm

Given the pH monitoring accuracy of ±4% and ±6% of pH reading in the basic and acidic conditions, respectively, GelDerm was previously shown to detect the emergence of wound infection (>10^5 CFU of Staphylococcus aureus and Pseudomonas aeruginosa) and monitor the change in bacterial density. Since wounds may experience temperature change due to circumstances such as infection, inflammation, and fever, the capability of the wound dressing to detect infection in a range of normal and pathological temperatures is crucial.[35] **Figure 2**A,C shows the performance of colorimetric pH sensors, the components that detect wound infection, in various temperatures. Results showed that temperature change from 34 to 40 °C did not exert any significant effect on the grayscale intensity change (p>0.11), and therefore, on the measured pH value. Sensor response time was also independent from the temperature (p>0.17) in pH values from 4 to 9, covering a wide range of potential infections manifested by acidic or basic wound pH. Therefore, the pH sensitivity of the wound dressing remained uninfluenced by the temperature change, leading to a consistent performance across physiological and pathological wound temperatures.

Furthermore, the impact of the storage time on the ability of the wound dressing to measure accurate pH values was assessed. As shown in Figure 2D,E, storing the wound dressings for 1 month at −20 °C did not significantly impact the accuracy of their pH sensors ($p \geq 0.98$) when exposed to buffers with various acidities. In contrast, storage for 3 months significantly impacted the grayscale intensity change ($p \leq 0.0452$) of the pH sensors, and therefore, a recalibration of the smartphone application is necessary to accurately detect the pH value when the wound dressing is stored for more than 1 month. As shown in Figure 1F, the impact of storage time was determined to be statistically significant on the sensor response time at target pH values of 7.4 and 9 ($p<0.01$ and $p<0.0097$, respectively). However, the pH response time remained under 35 min for all conditions.

To enhance the wound monitoring capability of GelDerm, 3D-printed glucose sensors were developed and integrated into the pH sensors to create an array of colorimetric pH-glucose screening modules (**Figure 3**A). These colorimetric sensors enabled the real-time monitoring of infection and glucose concentration in the wound, which is particularly beneficial for diabetic patients.[36–38] The glucose sensing function is based on an enzymatic reaction initiated by glucose oxidase used in these sensors. When glucose is introduced to the sensors, its oxidation and the reduction of oxygen generate oxygen peroxide, which leads to the oxidation of iodine to iodide by peroxidase, also used in the sensor, to yield a color change from light yellow (when glucose is absent) to dark red (when exposed to 12 mM of glucose), as shown in Figure 3B. The grayscale intensities of the photographs taken from the wound dressings that were incubated in aqueous glucose solutions were analyzed in red, green, and blue

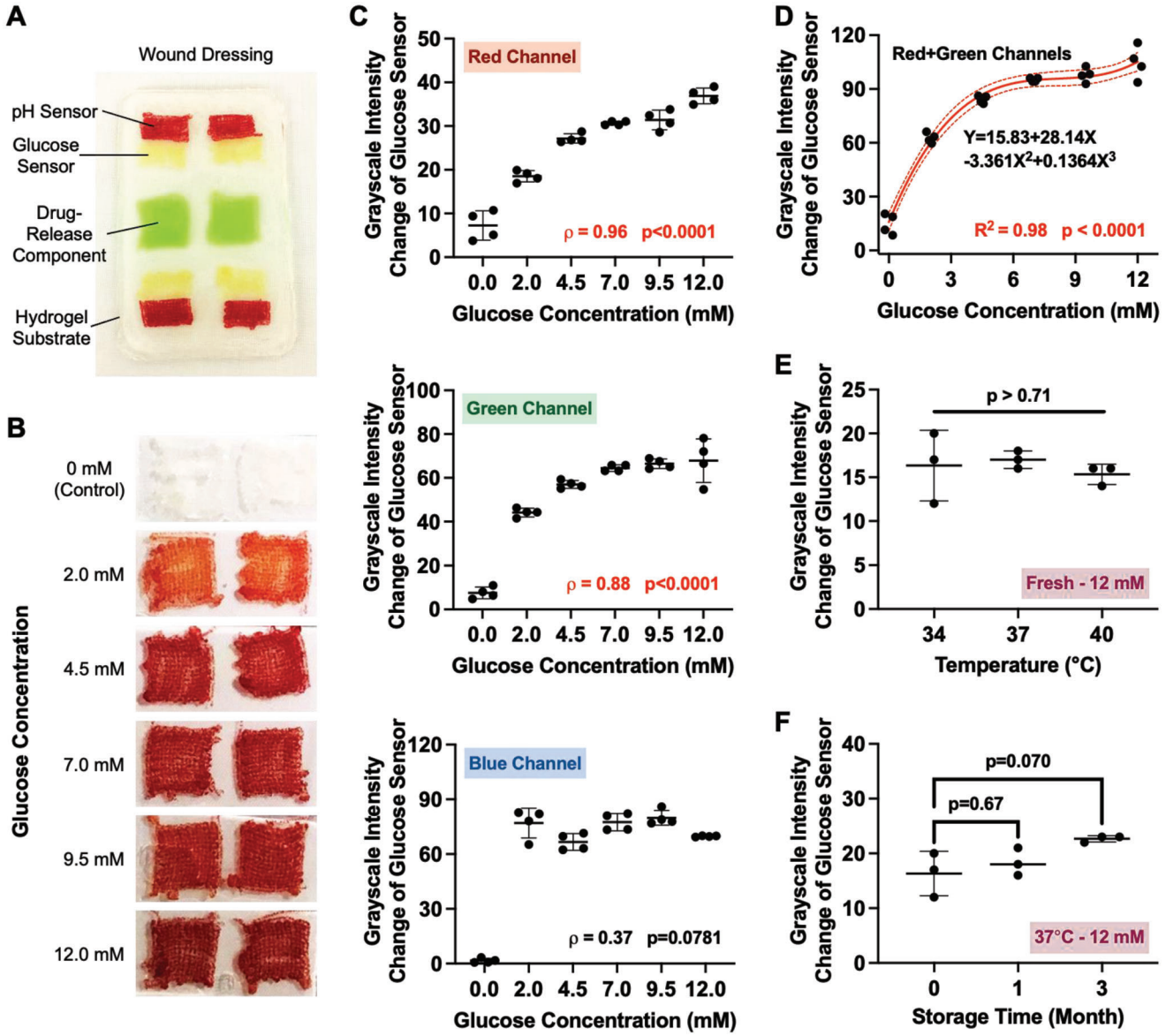

Figure 3. Incorporating glucose screening in GelDerm. A) In this version, GelDerm consists of an array of glucose and pH sensors to accommodate simultaneous, real-time glucose and infection monitoring. Here, the wound dressing was exposed to glucose (0.5 mM) so that its glucose sensors—transparent otherwise—became visible. B) The colorimetric glucose sensors changed color from white to dark red when exposed to glucose solutions with concentrations ranging from 0 to 12 mM. C) Grayscale intensity change of the glucose sensors in red, green, and blue channels as the glucose concentration increased. D) The standard curve, relating glucose concentration to the grayscale intensity change of the sensors. The solid line shows the standard curve; the dashed lines show the limits of the 95% confidence interval. E,F) The effect of temperature change (E) and storage time (F) on the grayscale intensity change of the glucose sensor. Error bars show mean ±SD. N = 4.

channels. As shown in Figure 3C, red and green channels showed increasing trends of grayscale intensity with glucose concentration with correlation coefficients of 0.96 and 0.88, respectively; however, the blue channel did not provide a significant statistical correlation with glucose concentration. To achieve a standard curve with greater correlation—relating the grayscale intensity and glucose concentration—the grayscale intensities of the red and green channels were added (Figure 3D). Based on the collective signals of red and green channels, the error of glucose sensing was determined to be within ±3% of the reading at glucose concentrations up to 4.5 mM, and this error gradually increased to ±10% at 12 mM of glucose. Notably, this level of accuracy is acceptable according to the FDA, which considers an accuracy of ±15% satisfactory for non-invasive glucose sensing. As blood glucose concentration is controlled below 10 mM in diabetic patients,[39] the tested sensible range of 0–12 mM will accommodate monitoring wound glucose levels in diabetic patients.

The impacts of temperature change and storage time on the performance of glucose sensors were also investigated. As shown in Figure 3E, change in temperature ranging from 34 to 40 °C did not significantly impact the change in the grayscale intensity of

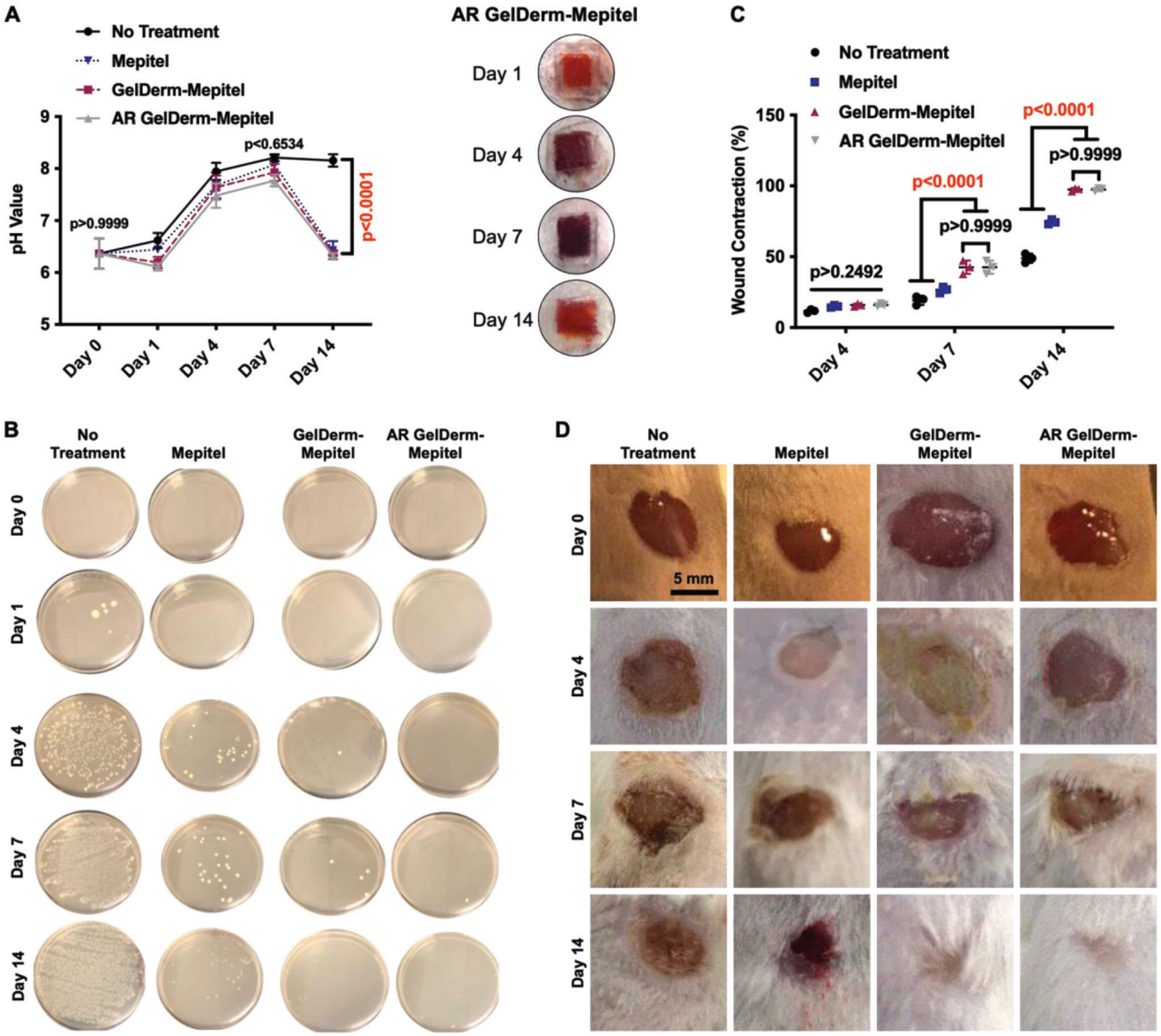

Figure 4. Evaluating the performance of GelDerm in the treatment of non-infected wounds in mouse models. A) pH changes in non-infected wounds in mouse models were measured using a commercial electrochemical pH probe. Four groups of treatments were considered: group 1, no treatment; group 2, treated with Mepitel alone; group 3, treated with GelDerm-Mepitel; group 4, treated with antibiotics-releasing (AR) GelDerm-Mepitel (GelDerm was loaded to gentamicin). B) Evaluating the bacterial barrier capability of GelDerm. At each time point, the dressing was removed from the wound and swab samples were collected and cultured on agar plates. C) Contraction of wounds in different treatment groups. D) Wound closure images in different treatment groups. Error bars show mean ±SD. N = 4.

the sensors (P>0.71) and therefore their detected glucose concentration. Similarly, storing the wound dressing at −20 °C for up to 3 months did not alter the performance of the sensors and their detected glucose concentration ($p \geq 0.070$), as shown in Figure 3F.

2.3. In Vivo Performance of GelDerm on Non-Infected Wounds

The in vitro results showed that GelDerm effectively provided real-time monitoring of the wound pH and glucose levels. The performance of GelDerm in terms of pH detection (infection monitoring), bacterial barrier properties, and wound contraction was further assessed in vivo. For this purpose, full-thickness 0.3-cm^2 wounds were excised on the back of mice and four groups of treatments were tested: 1) wounded mice without treatment, 2) wounded mice treated with GelDerm-Mepitel without drug delivery, 3) wounded mice treated with drug-releasing GelDerm-Mepitel, and 4) wounded mice treated with Mepitel only. This enabled us to identify the effects of GelDerm and the delivery of antibiotics on wound healing outcomes.

Figure 4A shows the wound pH, measured based on sensors' color change and image processing, that was collected on days 0,

1, 4, 7, and 14 post-injury. On day 1, the pH of the wounds was determined to be ≈6, close to the normal wound pH as reported previously.[40,41] During the initial stages of injury, the natural acidic environment of the wound can help reduce the surface microbial load, even if the pathogen is multi-resistant to antibiotics. On day 4 post-injury, the color of the sensors changed to dark red, indicating a pH increase in the wound, which was confirmed by measuring the actual wound pH. On day 14, the pH value of the wound in all GelDerm and Mepitel treated groups decreased to ≈6, which was an indication of complete wound healing; however, there was no observable decrease in pH in the untreated group.

One important role of a wound dressing is its ability to protect the wound environment from external pathogens to avoid infections and achieve rapid wound healing.[42] To assess the bacterial barrier properties of GelDerm, ESwabs were taken from wounds, in different treatment groups, and cultured on agar plates. As shown in Figure 4B, no clear colony of bacteria was observed on day 0, confirming the aseptic technique used during the surgery and the application of wound dressings. However, ESwab collected from the no-treatment group revealed the formation of bacterial colonies on day 1 and their proliferation over time, which is in agreement with the pH sensor readings shown in Figure 1A. Mild bacterial infection was also observed in wounds treated with Mepitel from day 4 to day 14. In contrast, during the course of the experiment, no clear bacterial colonies were observed for GelDerm-Mepitel and antibiotics-releasing GelDerm-Mepitel groups, showing GelDerm's ability to create a bacterial barrier and inhibit wound infection.

One of the important metrics to determine the healing efficacy of a wound dressing is its ability to accelerate wound contraction. As demonstrated in Figure 4C,D, wounds in all treatment groups contracted progressively with a similar rate within the first 4 days post injury. However, the wounds in the GelDerm-Mepitel and antibiotics-releasing GelDerm-Mepitel groups contracted at significantly higher rates after 7 days, showing a contraction of 42.65±3.56% and 49.13±3.08%, respectively. These contraction values were significantly higher than that of the Mepitel-treated and the control groups with 26.65±1.79% and 19.18±2.11% of wound contraction, respectively (p<0.0001). On day 14, wounds treated with GelDerm-Mepitel and antibiotics-releasing GelDerm-Mepitel were almost completely healed, while wounds with no treatment or treated with Mepitel became dehydrated with the formation of scabs. As expected, wounds treated with dressings containing antibiotics showed a better wound healing rate compared to all other groups, as antibiotics inhibited bacterial growth. These results confirmed the superior performance of GelDerm to accelerate wound healing compared to the commercially available Mepitel film. The better performance of GelDerm, as a hydrogel wound dressing, can be attributed to its ability to maintain wound moisture and regulate the wound exudates, which have been shown to stimulate tissue granulation and wound contraction.[43]

In addition to screening and antibiotics-releasing modules, the developed wound dressing was equipped with growth-factor-releasing components to accelerate the wound healing process. Benefiting from the spatial control provided by 3D printing, such drug-releasing components, as well as the pH and glucose sensors, can be deposited in a wide variety of patterns to accommodate the shape and size of the target wound.

In vitro release studies were conducted on both bFGF- and VEGF-loaded alginate fibers with various polymer concentrations. These release studies showed that an increase in the alginate concentration led to decreased release of the growth factor. As shown in **Figure 5**A, during 10 days of experiment, 65.9% ± 3.6% to 90.1% ± 10.0% of bFGF was released from alginate fibres with polymer concentrations from 16 wt% to 2 wt%. As shown in Figure 5B, hydrogel fibers composed of 2 wt.% and 16 wt.% of alginate released 71.3% ± 1.9% and 23.9% ± 1.5% of VEGF, respectively, during 10 days. Since the release behaviour of VEGF was highly dependent on the characteristics of the hydrogel barrier, release of this growth factor from hydrogel fibers embedded in the wound dressing was also studied. As shown in Figure 5C, the addition of the wound dressing barrier resulted in a significantly different release profile ($P = 0.0006$), decreasing the released amount of the growth factor from 71.3% ± 1.9% to 51.7% ± 2.8%.

Furthermore, the wound healing efficacy of GelDerm dressings loaded with VEGF, bFGF, and VEGF+bFGF was evaluated in wounded mouse models with 0.3 cm^2 of wound area. Figure 5D,E shows the representative wound images obtained for each treatment group at days 0, 4, 7, and 14 post injury along with the percentages of wound contraction over time. The results showed superior healing efficacy of GelDerm loaded with growth factors in comparison with that of blank GelDerm and no treatment groups. On days 4 and 7, treating the wound with VEGF+bFGF-loaded GelDerm led to a higher wound contraction compared to the other groups. Previous studies have found that dual or multiple deliveries of growth factors can significantly accelerate the wound healing process compared to their single delivery. This is due to the synergistic effects of boosting the stimulation of more cellular functions, including proliferation, migration, deposition of extracellular matrix, and the regulation of collagen synthesis.[44] Furthermore, on Day 7, the VEGF-treated wounds showed higher wound contraction (81.17±3.45%) compared to wounds treated with bFGF (66.38±4.78%). This can be attributed to the fact that VEGF triggers more effective biological functions in wound healing process, including the stimulation of angiogenesis, epidermal repair, and formation of granulation tissue,[45] while bFGF, mainly, promotes dermal fibroblast and keratinocyte migration and proliferation.[46] On day 14, all wounds treated with growth-factor-loaded GelDerm dressings completely healed, and no significant differences were found in the corresponding wound contraction. In contrast, wounds with no treatment or treated with blank GelDerm did not lead to complete wound closure and showed a significantly larger wound area.

2.4. In Vivo Performance of GelDerm on Infected Wounds

Once the skin surface is impaired, microorganisms common to the normal skin flora, as well as exogenous bacteria and fungi, gain access to the underlying tissues, which provides a favorable environment for their growth and development. This issue is exacerbated when healing is delayed, as the normal microbiota of the wound changes and more aggressive pathogens

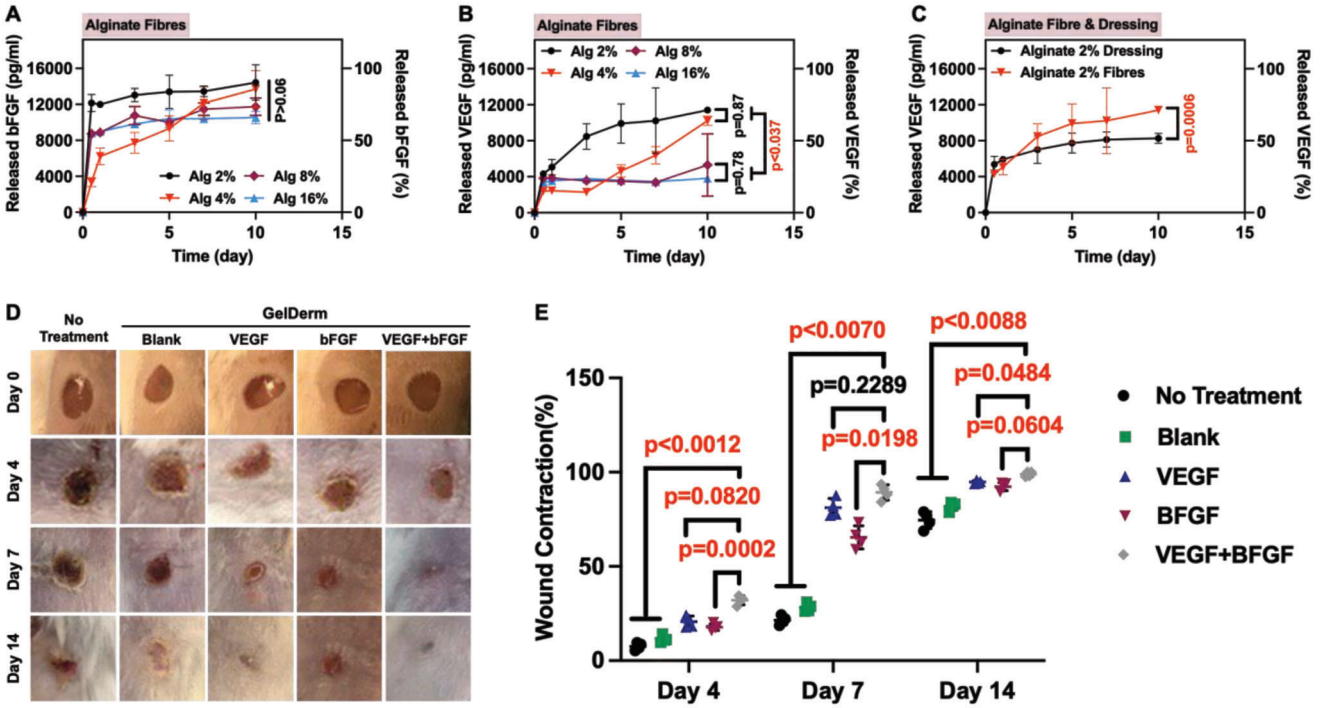

Figure 5. The effect of GelDerm's growth factor delivery module on the wound healing process. A) The release of bFGF from hydrogel fibers composed of alginate with concentrations of 2 wt.% to 16 wt.%. B) The release of VEGF from hydrogel fibers composed of alginate with concentrations ranging from 2 wt.% to 16 wt.%. C) The release profile of VEGF from hydrogel fibers made of 2 wt.% alginate in two different conditions: non-embedded and embedded in hydrogel wound dressing composed of 2 wt.% alginate. D) Photographic images showing the effect of growth-factor-loaded GelDerm on wound closure in non-infected wounds in mouse models. E) Quantification of wound contraction in non-infected wounds with no treatment and treated with blank wound dressing as well as wound dressing loaded with VEGF, bFGF, and VEGF+bFGF over 14 days. Error bars show mean ±SD. N = 4.

can reside in the wound environment.[47] It has been shown that bacterial counts of 10^5 CFU g^{-1} and higher in the wound environment cause infection complications.[48,49] Here, the efficacy of GelDerm in the treatment of 0.3-cm^2 wounds infected with *E. coli* at concentrations of 10^4, 10^6, and 10^8 CFU mL^{-1} was evaluated. When such wounds remained untreated, an increase in the initial concentration of *E. coli* significantly delayed the wound contraction (Figure S3, Supporting Information) and led to increased bacterial growth in the wound area over time (Figure S4, Supporting Information). **Figure 6**A shows the variation of wound pH under various degrees of bacterial infection over 7 days; wounds infected with 10^8 CFU mL^{-1} showed a significantly higher pH (9.2±0.2) compared to non-infected wounds and those inoculated with 10^4 and 10^6 CFU mL^{-1} after 7 days (7.7 to 8.2; $p = 0.002$). As shown in Figure 6B, treatment with Mepitel-antibiotics and antibiotics-releasing GelDerm-Mepitel led to a significant decrease in the wound pH, measured by a pH probe, after 7 days ($p = 0.0001$), which is an indication of wound healing and reduction of bacterial growth. The pH change was also captured by the pH sensors, as they responded to the pH variation by changing color. As shown in Figure 6C, this was evident when infected wounds were treated with blank and antibiotics-releasing GelDerm. On day 1 post infection, higher pH values were observed in infected wounds with an initial inoculation of 10^8 CFU mL^{-1} for both treatment groups. Wounds with severer initial infection and treated with antibiotics-releasing GelDerm exhibited an increasing trend of pH from day 1 to day 4 (7.1±0.2 to 7.9±0.2) and decreasing trend afterwards, showing an average pH of 7.5±0.1 on day 7. In contrast, wounds with the same initial infection severity, but treated with blank dressings, showed increasing pH values throughout the study, reaching a pH of 9.1±0.2 on day 7, which can be attributed to bacterial growth.[50] This pH change behavior observed by GelDerm's pH sensors was consistent with the previous measurement performed by the pH probe (Figure 6B), which validates the capability of GelDerm to identify and monitor infection in a real-time manner with sensitivity to bacterial concentration and growth.

To assess the ability of GelDerm in the treatment of infected wounds, those infected with an initial bacteria concentration of 10^8 CFU mL^{-1} were studied under four different treatment conditions: no treatment and treatment with GelDerm-Mepitel, Mepitel-antibiotics, and antibiotics-releasing GelDerm-Mepitel over 7 days. As shown in Figure 6D,E, wounds treated with antibiotics-releasing GelDerm-Mepitel started healing at a significantly higher rate by showing significantly higher contraction on day 4 ($p<0.0389$). This effect was more pronounced on day 7, when infected wounds showed an average contraction of 16%±2%, which was significantly higher ($p<0.0076$) than those with no treatment (5%±2%) and treated with blank GelDerm (9%±1%). Additionally, wound contraction under treatment with antibiotics releasing GelDerm was determined to be slightly higher than treatment with Mepitel-antibiotics (16%±2% vs 15%±2%).

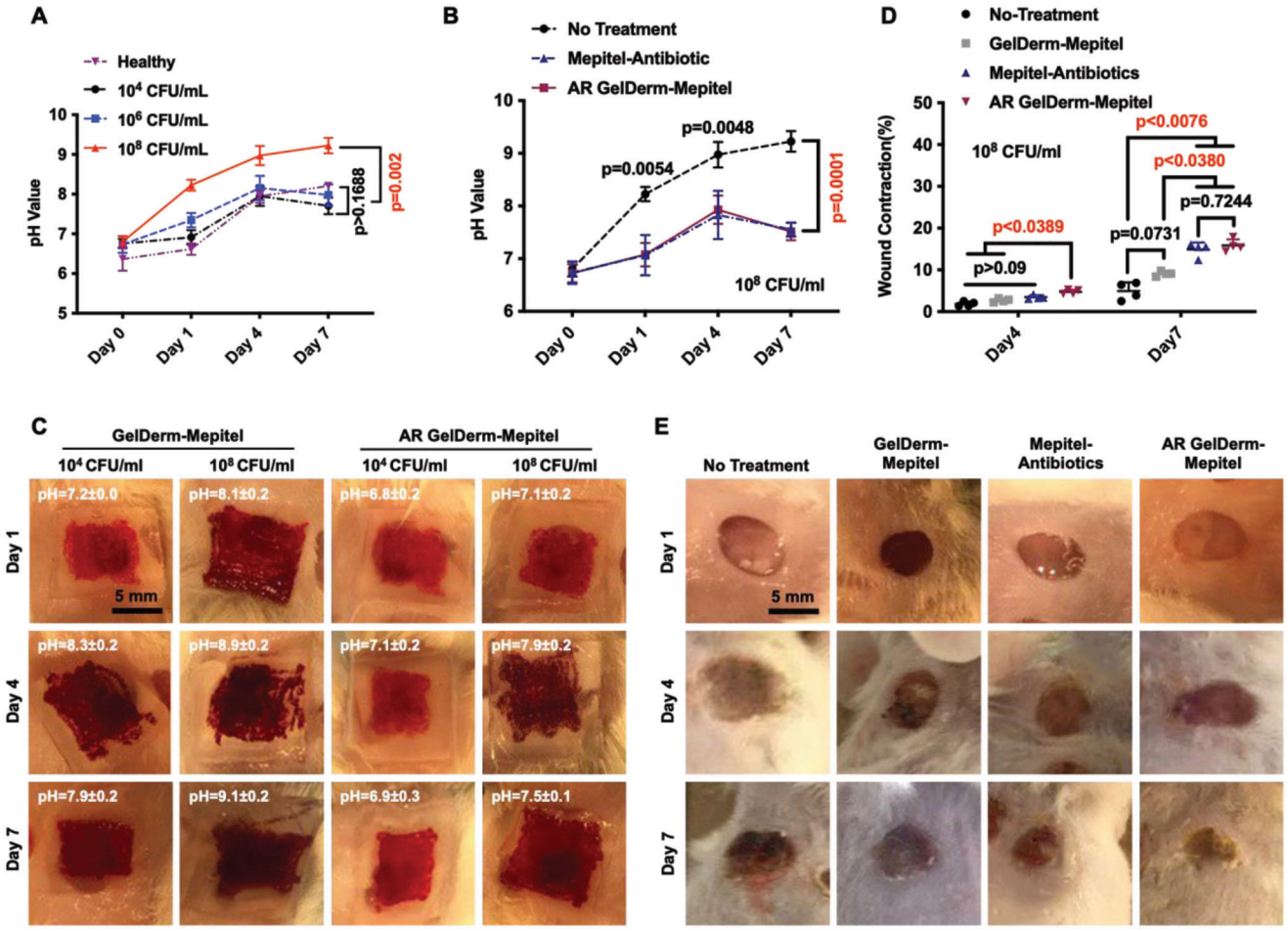

Figure 6. Evaluating the performance of GelDerm in the treatment of infected wound models. A) pH variation in infected wounds, inoculated with different densities of E. Coli, over time. B) pH change in infected wounds (initially inoculated with 10^8 CFU mL^{-1}) and treated with antibiotics-releasing (AR) GelDerm and Mepitel-antibiotics. C) GelDerm's pH sensors responded to the variations of pH, correlated to bacterial infection, in wounds treated with AR and blank wound dressings. D) Contraction of infected wounds (initially inoculated with 10^8 CFU mL^{-1}) with various treatments over time. E) Photographs showing the status of infected wounds treated in various conditions over time. Error bars show mean ±SD. N = 4.

Furthermore, the effect of subject sex on the wound healing rate of infected wounds, treated with antibiotics, was studied. As shown in Figure S5, Supporting Information, while both female and male mouse models responded to the antibiotics and showed increased wound contraction compared to the no-treatment group, males exhibited a higher healing rate and better response to the antibiotics. This phenomenon can be attributed to the difference in hormones between male and female animals. In contrast, sex did not have any significant impact on the wound pH change (Figure S6, Supporting Information). Therefore, GelDerm can be deemed capable of wound infection monitoring for both male and female subjects.

2.5. Histopathological Analysis

Histopathological staining methods, including hematoxylin and eosin (H&E) and Masson's trichrome (MT), were used to investigate the effect of GelDerm on the healing process of infected wound models for 14 days. Observed by H&E, wounds that received no treatment displayed infiltration of inflammatory cells, dermis damage, and epidermal detachment after 7 days (**Figure 7**A). Signs of mild macrophage and neutrophil infiltrations were also observed in wounds treated with blank GelDerm-Mepitel; however, those treated with antibiotics-releasing GelDerm-Mepitel exhibited epidermis regeneration, formation of blood capillaries, and granulation, evident with the proliferation of fibroblasts, with much fewer inflammatory cell infiltration. After 14 days, all treatment groups showed epidermis regeneration with increased thickness compared to day 7. Wounds treated with antibiotics-releasing GelDerm-Mepitel showed the largest healing zone and regenerated epidermis thickness, a higher level of ECM secretion, a greater number of hair follicle cells and sebaceous glands, and minimum inflammatory cell infiltration compared to the other treatment groups. In contrast, untreated wounds showed the highest inflammatory cell infiltration and the minimum newly formed hair follicles, blood vessels, and sebaceous glands. Interestingly, the formation

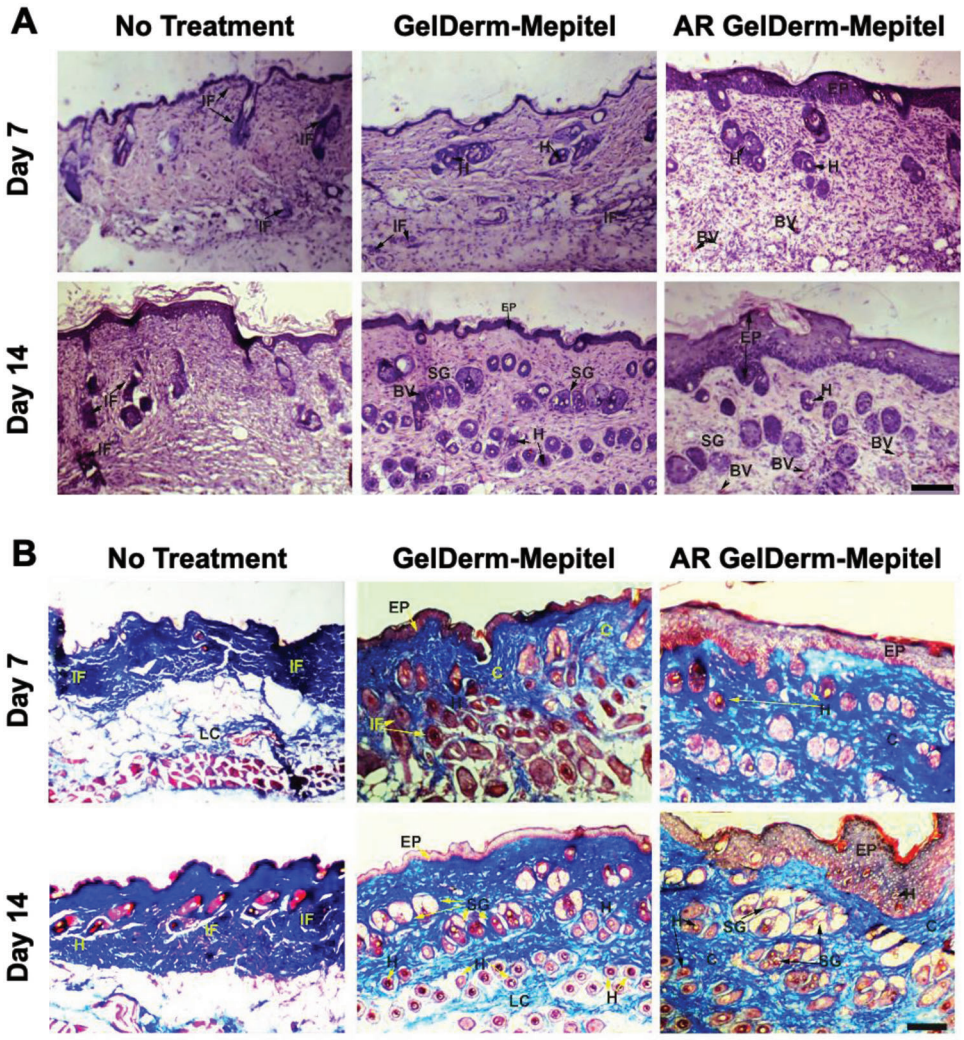

Figure 7. Histopathological analysis of infected wounds treated with GelDerm. A) Hematoxylin and eosin (H&E) histopathological images of the wounds treated in different groups—no treatment and treatment GelDerm-Mepitel or antibiotics-releasing (AR) GelDerm-Mepitel—after 7 and 14 days of treatment (EP: regenerated epidermis; H: hair follicles; BV: blood vessels; IF: inflammatory cells, scale bar = 50 μm). B) The Masson's trichrome (MT) histopathological images of the wounds covered with different groups after 7 and 14 days of treatment (EP: regenerated epidermis; H: hair follicles; IF: inflammatory cells, C: collagen, LC: loose collagen; scale bar = 50 μm).

of many new blood vessels, which is essential for the continuation of the healing process, was observed in the wounds treated with blank GelDerm.

Wound healing is highly dependent on the synthesis of collagen as the main content of skin ECM. Therefore, MT staining was performed to further evaluate the effect of GelDerm on wound healing. As demonstrated in Figure 7B, collagen deposition (shown in blue), which is a sign of ECM organization, was noticeable in larger areas in both GelDerm-treated groups compared to the no-treatment group on days 7 and 14. Especially, clusters of collagen fibers were observed in the newly formed granulation tissue in wounds treated with antibiotics-releasing GelDerm-Mepitel after 14 days. Overall, as evident by both histopathological analyses, treatment with GelDerm, especially when loaded with antibiotics, resulted in reduced hypertrophic scarring and inflammation, larger epidermal thickness, and an accelerated healing process, which is in agreement with the results presented in Figure 6.

3. Conclusion

In this study, we further improved the screening and therapeutic capabilities of our previously developed smart wound dressings, GelDerm, by incorporating glucose sensors and antibiotics/growth factor-releasing modulus. GelDerm's colorimetric pH sensors were shown effective in monitoring wound infection with suitable sensitivity to the severity of infection in male and female mouse models. It was also shown that these sensors perform accurately in various temperatures and after 1 month of storage. GelDerm functioned as a pathogen barrier and reduced the risk of infection in the wound models. Additionally, via delivering antibiotics and growth factors, this wound dressing

demonstrated superior performance in accelerating the healing process in both infected and non-infected wounds. In multiple experiments, the performance of GelDerm was compared with the commercially available Mepitel film, with and without the application of antibiotics, in which GelDerm showed either significantly better performance (when growth factor was used for the treatment of non-infected wounds) or slightly better performance (when antibiotics were delivered for the treatment of infected wounds). In particular, GelDerm is compatible with Mepitel film, which provides effective adherence and conformal contact to the wound area. As a future direction, this dressing will be tested on infected wounds in diabetic subjects to evaluate its monitoring and drug delivery features in more complex wound environments.

4. Experimental Section

Glucose-Sensitive Beads: A glucose-sensitive solution was prepared by dissolving 6 mg of glucose oxidase (cat: G2133, Sigma-Aldrich, St. Louis, USA), 0.6 mg of horseradish peroxidase (cat: SRE0082, Sigma-Aldrich, St. Louis, USA), 498 mg of potassium iodide (cat: 221945, Sigma-Aldrich, St. Louis, USA), and 513 mg of trehalose (cat: PHR1344, Sigma-Aldrich, St. Louis, USA) in 5 mL of sodium citrate (cat: BDH9288, VWR, Radnor, USA) buffer (pH 6).[51–53] Next, 2000 mg of Dowex 1 × 4 chloride foam beads (Sigma-Aldrich, St. Louis, USA) were washed 3 times with deionized (DI) water and once with anhydrous ethanol. Following, ethanol was aspirated and replaced with the glucose-sensitive solution and incubated at 4 °C overnight to allow the dye to conjugate to the beads. The solution was aspirated, and the beads were washed with DI water 4 times, leaving the glucose-sensitive beads (Figure S7A, Supporting Information).

Glucose-Sensitive Sensors: The prepared glucose-sensitive beads were added to 4% (w/v) aqueous sodium alginate (SKU: 71238, Sigma-Aldrich, St. Louis, USA) solution and vortex-mixed to achieve a uniform suspension. This polymeric suspension along with 6% (w/v) $CaCl_2$ (Cat: CT1330, Bio Basic, Markham, Canada) solution was used in a coaxial extruder system, as described previously,[7,8] to print hydrogel fibers. The fibers were 3D-printed and arranged into 2-layer rectangular structures, forming the glucose sensors (Figure S7B, Supporting Information).

Evaluating the Performance of pH and Glucose Sensors: Hydrogel sensors were incubated in different media—pH sensors in buffers with known pH and glucose sensors in glucose solutions with known concentrations—at specified temperatures. The sensors were monitored by a GoPro camera (HERO 7, San Mateo, USA) with photographs taken over time (Figure 7C). Red, green, and blue (RGB) channels of each image were split and converted to grayscale format using ImageJ software.[7,8] The change in the grayscale intensity of each sensor was measured over time to achieve a standard curve, correlating grayscale intensity and the measured parameter, pH, or glucose concentration. The response time of a sensor was considered the duration of time in which the sensor achieved 90% of its final grayscale intensity.

Fabrication of Growth-Factor-Loaded Hydrogel Structures: Each type of growth factor—human bFGF 154 aa (cat: 100–18B, PeproTech, Rocky Hill, USA) or VEGF 165 (100–20, PeproTech, Rocky Hill, USA)—was separately dissolved in DI water to reach a concentration of 500 ng mL^{-1}. Per each µg of growth factor, 2.2 mg of bovine serum albumin (BSA) (cat: A2153, Sigma-Aldrich, St. Louis, USA) and 25 µg of heparin sodium salt (cat: H3393, Sigma-Aldrich, St. Louis, USA) were added to both growth factor solutions. Following, sodium alginate was added to the solutions to reach wt.% concentrations of 2%, 4%, 8%, or 16%. An ionic crosslinking method with a 6-wt% $CaCl_2$ solution and a coaxial extruder, as described before,[7,8,54] was used to 3D-print fibrous hydrogel structures from the polymeric growth factor solutions with 2 wt.% and 4 wt.% of alginate. A different ionic crosslinking method with a single-channel extruder and a 6 wt.% $CaCl_2$ bath, as previously described,[55] was used to 3D-print growth factor solutions with 8 wt.% or 16 wt.% alginate. The growth-factor-loaded hydrogel fibers were 3D printed and arranged into 2-layer structures. The concentration of alginate—ranging from 2% (w/v) to 16% (w/v)—in these drug-releasing components was used to tune the drug release profile, as shown in Figure 5A. In the wound dressings used for the in vivo study, the concentration of alginate for bFGF- and VEGF-loaded scaffolds was set to 4% (w/v) and 2% (w/v), respectively.

Release Study on Growth-Factor-Loaded Hydrogel Structures: A BSA solution with a concentration of 35.5 mg mL^{-1} in 0.1 M Tris buffer (cat: T6066, Sigma-Aldrich, St Louis, USA) with a pH of 7.4 was used as the release medium. 10 µL of 3D-printed fiber containing each type of growth factor was suspended in 300 µL of the release medium and incubated at 37 °C. At each time point, 20 µL of the supernatant was collected, frozen at −20 °C, and replaced with 20 µL of fresh release medium. Supernatants were analyzed with a bFGF ELISA kit (900-K08) or a VEGF ELISA kit (900-K10). The ELISA well-plates were measured via spectrophotometry using a microplate reader (Infinite 200 Pro, Tecan, männedorf, Switzerland).

Fabrication of Wound Dressings: An array of glucose and pH sensors was printed into a rectangular cavity that served as a mold to cast the wound dressing (Figure S8A, Supporting Information). The drug-releasing components were placed into the mold. Alginate 2% (w/v) solution was dispensed into the mold and cross-linked with $CaCl_2$ 6% (w/v) vapor (Figure S8B, Supporting Information). Wound dressings were sterilized using ultraviolet light (4 µW cm^{-2}) irradiation for 45 min on each side and tested on murine-infected wound models (Figure S8C, Supporting Information). Antibiotics-loaded wound dressings were fabricated using two methods: 1) gentamicin sulfate was dissolved in the alginate solution (for the main body of the wound dressing) at a concentration of 3 mg mL^{-1} before casting, or 2) a 3D printed alginate scaffold containing 2% (w/v) alginate and 3 mg mL^{-1} gentamicin was incorporated into the wound dressing. For the in vivo tests in mouse models, the second method was used.

In Vivo Studies: All experiments were performed using adult male and female BALB/c mouse models, weighing 20 to 30 grams. All animals were housed in individual cages under constant temperature (22 °C) and humidity, with a 12-h light/dark cycle. Animals had access to sterile food and water as desired throughout the study. The study was approved by the Animal Research Ethics Committee at the University of Victoria (Protocol number: 2018–021(1)). All mice were anesthetized by inhalation of isoflurane. Buprenorphine at 0.05 mg kg^{-1} (Hospira Inc., Lake Forest, IL) was given via injection for pain management. The dorsal surface of the animals was shaved using electric clippers and dried. Two full-thickness wounds, overlying the thoracic spinal column and the adjacent musculature, were induced using a biopsy punch (6 mm, Integra Miltex) on each animal. The mice were then randomly divided into 8 groups as follows: without treatment and treated with Mepitel, GelDerm-Mepitel, antibiotics releasing GelDerm-Mepitel, VEGF-releasing GelDerm-Mepitel, bFGF-releasing GelDerm-Mepitel, VEGF+bFGF-releasing GelDerm-Mepitel. For securely fixing the GelDerm hydrogels on the wound area, a rectangular section (30 mm by 30 mm) of transparent dressing (Mepitel; Molnlycke Safetac) was placed over the GelDerm and secured with tissue adhesive (Vetbond).

For the inoculation of infection in the wounded mice, aliquots of 25 µL broth suspension containing different concentrations of *E. Coli* (10^4, 10^6, or 10^8 CFU mL^{-1}) were pipetted into the surface of the wound and allowed to absorb for 3 min. The mice were then randomly divided into 6 groups as follows: without treatment and treated with Mepitel-antibiotics, GelDerm, and antibiotics-releasing GelDerm-Mepitel. The wound dressings were changed every 4 days. After days 4, 7, and 14, the wound dressings were removed, and wound closure was calculated using:

$$\text{Wound closure } (\%) = \frac{A_0 - A_t}{A_0} \times 100 \quad (1)$$

where A_0 and A_t are the initial wound area and the wound area at time t, respectively. Afterwards, the mice were sacrificed via cervical dislocation and the wound tissue was harvested for further pathological investigation.

pH Measurements of the Wounds: At each time point, the wound pH was determined using previously developed thread-based pH sensors.[56]

Bacterial Analysis: On days 1, 4, and 7 post-infection, the wound dressings were removed and the wound site was swabbed using ESwab (COPAN Diagnostic Inc.). Collected samples were cultured on agar plates to determine the number of bacteria. Macroscopic images of each test group were taken with a digital camera to quantify the level of infection.

Histopathological Analysis: Wound tissue sections were collected on days 7 and 14, fixed with formalin (10%), and embedded in paraffin. Embedded samples were sectioned with 4 µm of thickness, de-paraffinized, and stained with H&E or MT. The stained sections were observed with a light microscope (Olympus BX51).

Statistical Analysis and Graphing: Pooled t-test or one-way analysis of variance with Tukey–Kramer HSD test was used to perform the comparison between pairs of experimental data with 2 or more than 2 groups with equal variance, respectively. Welch's ANOVA test was used to compare groups of experimental data with unequal variance. The arithmetic mean and standard deviation (SD) were used to express the central tendency and variation of samples, respectively. All statistical analyses were performed using JMP Pro 14 software. All graphs were generated using Prism 8 software.

Supporting Information

Supporting Information is available from the Wiley Online Library or from the author.

Acknowledgements

B.M. and Z.H. contributed equally to this work. M.A., B.M., Z.H., and S.M.H.D. acknowledge the funding received from the Natural Sciences and Engineering Research Council of Canada (NSERC) discovery grant. M. A. and Z. H. acknowledge the seed funding received from the International Collaboration on Repair Discoveries (ICORD). This study is partially supported by the National Institute of Health, National Institute of Diabetes and Digestive and Kidney Diseases (award number 1R01124789-01A1) to D. G. A.

Conflict of Interest

The authors declare no conflict of interest.

Data Availability Statement

The data that support the findings of this study are available from the corresponding author upon reasonable request.

Keywords

biomaterials, biosensing, chronic wounds, smart dressings, wound management

Received: December 12, 2022
Revised: February 24, 2023
Published online: March 29, 2023

[1] C. Lindholm, R. Searle, *Int. Wound J.* **2016**, *13*, 5.
[2] C. K. Sen, G. M. Gordillo, S. Roy, R. Kirsner, L. Lambert, T. K. Hunt, F. Gottrup, G. C. Gurtner, M. T. Longaker, *Wound Repair Regener.* **2009**, *17*, 763.
[3] L. Martinengo, M. Olsson, R. Bajpai, M. Soljak, Z. Upton, A. Schmidtchen, J. Car, K. Järbrink, *Ann. Epidemiol.* **2019**, *29*, 8.
[4] K. Heyer, K. Herberger, K. Protz, G. Glaeske, M. Augustin, *Wound Repair Regener.* **2016**, *24*, 434.
[5] A. Mehrabi, H. Fonouni, M. Wente, M. Sadeghi, C. Eisenbach, J. Encke, B. M. Schmied, M. Libicher, M. Zeier, J. Weitz, M. W. Büchler, J. Schmidt, *Clin. Transplant.* **2006**, *20*, 97.
[6] D. Church, S. Elsayed, O. Reid, B. Winston, R. Lindsay, *Clin. Microbiol. Rev.* **2006**, *19*, 403.
[7] B. Mirani, E. Pagan, B. Currie, M. A. Siddiqui, R. Hosseinzadeh, P. Mostafalu, Y. S. Zhang, A. Ghahary, M. Akbari, *Adv. Healthcare Mater.* **2017**, *6*, 1700718.
[8] B. Mirani, *Development of a multifunctional dressing for epidermal wound monitoring and on-site drug delivery*, University of Victoria, Victoria, BC V8P 5C2, Canada, **2017**.
[9] P. Salvo, N. Calisi, B. Melai, V. Dini, C. Paoletti, T. Lomonaco, A. Pucci, F. Di Francesco, A. Piaggesi, M. Romanelli, *Int. J. Nanomed.* **2017**, *12*, 949.
[10] Q. Pang, D. Lou, S. Li, G. Wang, B. Qiao, S. Dong, L. Ma, C. Gao, Z. Wu, *Adv. Sci.* **2020**, *7*, 1902673.
[11] P. Mostafalu, W. Lenk, M. R. Dokmeci, B. Ziaie, A. Khademhosseini, S. R. Sonkusale, *IEEE Trans. Biomed. Circuits Syst.* **2015**, *9*, 670.
[12] Z. Li, E. Roussakis, P. G. L. Koolen, A. M. S. Ibrahim, K. Kim, L. F. Rose, J. Wu, A. J. Nichols, Y. Baek, R. Birngruber, G. Apiou-Sbirlea, R. Matyal, T. Huang, R. Chan, S. J. Lin, C. L. Evans, *Biomed. Opt. Express* **2014**, *5*, 3748.
[13] D. A. Jankowska, M. B. Bannwarth, C. Schulenburg, G. Faccio, K. Maniura-Weber, R. M. Rossi, L. Scherer, M. Richter, L. F. Boesel, *Biosens. Bioelectron.* **2017**, *87*, 312.
[14] D. Sharp, S. Forsythe, J. Davis, *J. Biochem.* **2008**, *144*, 87.
[15] D. Sharp, P. Gladstone, R. B. Smith, S. Forsythe, J. Davis, *Bioelectrochemistry* **2010**, *77*, 114.
[16] A. Mclister, J. Phair, J. Cundell, J. Davis, *Electrochem. Commun.* **2014**, *40*, 96.
[17] T. R. Dargaville, B. L. Farrugia, J. A. Broadbent, S. Pace, Z. Upton, N. H. Voelcker, *Biosens. Bioelectron.* **2013**, *41*, 30.
[18] C. Pak, J. In Jeon, H. Kim, J. Kim, S. Park, K. -H. Ahn, Y. -J. Son, S. Yoo, R. -M. Baek, J. H. Jeong, C. Y. Heo, *Wound Repair Regener.* **2018**, *26*, S19.
[19] P. Kassal, J. Kim, R. Kumar, W. R. De Araujo, I. M. Steinberg, M. D. Steinberg, J. Wang, *Electrochem. Commun.* **2015**, *56*, 6.
[20] H. Derakhshandeh, S. S. Kashaf, F. Aghabaglou, I. O. Ghanavati, A. Tamayol, *Trends Biotechnol.* **2018**, *36*, 1259.
[21] P. Bao, A. Kodra, M. Tomic-Canic, M. S. Golinko, H. P. Ehrlich, H. Brem, *J. Surg. Res.* **2009**, *153*, 347.
[22] P. Losi, E. Briganti, C. Errico, A. Lisella, E. Sanguinetti, F. Chiellini, G. Soldani, *Acta Biomater.* **2013**, *9*, 7814.
[23] S. Kanazawa, T. Fujiwara, S. Matsuzaki, K. Shingaki, M. Taniguchi, S. Miyata, M. Tohyama, Y. Sakai, K. Yano, K. Hosokawa, T. Kubo, *PLoS One* **2010**, *5*, e12228.
[24] M. Miyoshi, T. Kawazoe, H. H. Igawa, Y. Tabata, Y. Ikada, S. Suzuki, *J. Biomater. Sci., Polym. Ed.* **2005**, *16*, 893.
[25] Y. Sogabe, M. Abe, Y. Yokoyama, O. Ishikawa, *Wound Repair Regener.* **2006**, *14*, 457.
[26] S. Constantino Rosa Santos, C. Miguel, I. Domingues, A. Calado, Z. Zhu, Y. Wu, S. Dias, *Exp. Cell Res.* **2007**, *313*, 1561.
[27] L. Gan, P. Fagerholm, J. Palmblad, *Acta Ophthalmol. Scand.* **2004**, *82*, 557.
[28] N. J. Trengove, M. C. Stacey, S. Macauley, N. Bennett, J. Gibson, F. Burslem, G. Murphy, G. Schultz, *Wound Repair Regener.* **1999**, *7*, 442.
[29] M. Akbari, B. Mirani, A. Ghahary, M. A. Siddiqui, *Patent Cooperation Treaty (PCT/IB2018/053491)*, **2018**.
[30] R. Dong, B. Guo, *Nano Today* **2021**, *41*, 101290.
[31] M. Farahani, A. Shafiee, *Adv. Healthcare Mater.* **2021**, *10*, 2100477.
[32] Q. Zeng, X. Qi, G. Shi, M. Zhang, H. Haick, *ACS Nano* **2022**, *16*, 1708.

[33] A. Kar, N. Ahamad, M. Dewani, L. Awasthi, R. Patil, R. Banerjee, *Biomaterials* **2022**, *283*, 121435.
[34] M. Tan, Y. Xu, Z. Gao, T. Yuan, Q. Liu, R. Yang, B. Zhang, L. Peng, *Adv. Mater.* **2022**, *34*, 2108491.
[35] A. Chanmugam, D. Langemo, K. Thomason, J. Haan, E. A. Altenburger, A. Tippett, L. Henderson, T. A. Zortman, *Adv. Skin Wound Care* **2017**, *30*, 406.
[36] J. T. King, J. L. Goulet, M. F. Perkal, R. A. Rosenthal, *Ann. Surg.* **2011**, *253*, 158.
[37] K. J. Zerr, A. P. Furnary, G. L. Grunkemeier, S. Bookin, V. Kanhere, A. Starr, *Ann. Thoracic Surge.* **1997**, *63*, 356.
[38] S. C.-S. Hu, C.-C. E. Lan, *J. Dermatol. Sci.* **2016**, *84*, 121.
[39] M. Egi, R. Bellomo, E. Stachowski, C. J. French, G. K. Hart, C. Hegarty, M. Bailey, *Crit. Care Med.* **2008**, *36*, 2249.
[40] L. A. Schneider, A. Korber, S. Grabbe, J. Dissemond, *Arch. Dermatol. Res.* **2007**, *298*, 413.
[41] S. Bagherifard, A. Tamayol, P. Mostafalu, M. Akbari, M. Comotto, N. Annabi, M. Ghaderi, S. Sonkusale, M. R. Dokmeci, A. Khademhosseini, *Adv. Healthcare Mater.* **2016**, *5*, 175.
[42] H. Ameen, K. Moore, J. C. Lawrence, K. G. Harding, *J. Wound Care* **2000**, *9*, 385.
[43] A. Sood, M. S. Granick, N. L. Tomaselli, *Adv. Wound Care* **2014**, *3*, 511.
[44] U. Park, K. Kim, *Biotechnol. Bioprocess Eng.* **2017**, *22*, 659.
[45] K. E. Johnson, T. A. Wilgus, *Adv. Wound Care* **2014**, *3*, 647.
[46] S. Akita, K. Akino, A. Hirano, *Adv. Wound Care* **2013**, *2*, 44.
[47] R. Serra, R. Grande, L. Butrico, A. Rossi, U. F. Settimio, B. Caroleo, B. Amato, L. Gallelli, S. De Franciscis, *Expert Rev. Anti-Infect. Ther.* **2015**, *13*, 605.
[48] P. G. Bowler, B. I. Duerden, D. G. Armstrong, *Clin. Microbiol. Rev.* **2001**, *14*, 244.
[49] A. R. Siddiqui, J. M. Bernstein, *Clin. Dermatol.* **2010**, *28*, 519.
[50] G. Stüttgen, H. Schaefer, *Funktionelle dermatologie: grundlagen der morphokinetik pathophysiologie, pharmakoanalyse und therapie von dermatosen*, Springer-Verlag, Berlin, Germany, **2013**.
[51] A. Koh, D. Kang, Y. Xue, S. Lee, R. M. Pielak, J. Kim, T. Hwang, S. Min, A. Banks, P. Bastien, M. C. Manco, L. Wang, K. R. Ammann, K.-I. Jang, P. Won, S. Han, R. Ghaffari, U. Paik, M. J. Slepian, G. Balooch, Y. Huang, J. A. Rogers, *Sci. Transl. Med.* **2016**, *8*, 366ra165.
[52] A. W. Martinez, S. T. Phillips, M. J. Butte, G. M. Whitesides, *Angew. Chem.* **2007**, *119*, 1340.
[53] A. W. Martinez, S. T. Phillips, E. Carrilho, S. W. Thomas, H. Sindi, G. M. Whitesides, *Anal. Chem.* **2008**, *80*, 3699.
[54] B. Mirani, E. Pagan, S. Shojaei, J. Duchscherer, B. D. Toyota, S. Ghavami, M. Akbari, *Eur. J. Pharmacol.* **2019**, *854*, 201.
[55] R. Hosseinzadeh, B. Mirani, E. Pagan, S. Mirzaaghaei, A. Nasimian, P. Kawalec, S. C. Silva Rosa, D. Hamdi, N. P. Fernandez, B. D. Toyota, J. W. Gordon, S. Ghavami, M. Akbari, *Adv. Ther.* **2019**, *2*, 1900113.
[56] L. Karperien, S. M. H. Dabiri, Z. Hadisi, D. Hamdi, E. Samiei, M. Akbari, in *2019 IEEE International Flexible Electronics Technology Conference (IFETC)*, IEEE, Vancouver, Canada, pp. 1–5.